A Moving Lagrangian Mesh Model of a Lava Dome Volcano and Talus Slope

Dr. Nick Robertson

Department of Mathematics

Reading University, UK

August 21, 2006

Declaration:

I confirm that this work is my own and the use of all other material from other sources has been properly and fully acknowledged.

Nick Robertson

Acknowledgments

First I would like to acknowledge the EPSRC for allowing me the opportunity to study this course and fund this research.

Contents

Abstract

Two height averaged expanding Lagrangian mesh models are developed of a lava dome volcano and it's attached talus slope; the first is a simple slab geometry while the second is axi-symmetric. The models are developed in C++ using an object orientated class frame-work.

The Rheology of the lava is modelled in the dome and the talus is fixed by geometric geological observations. Material is extruded into the dome from a volcanic conduit and the model allowed to calculate the expansion of the Lagrangian cells based on the rheological flow of the lava. A conservation law determines the amount of material distributed into the dome and the talus iteratively for each time step.

The slab model is seen to produce results which are compatible with geological observations and previous studies, these however, do not include a talus. The radial model is observed to require further work; several suggestions are made.

Figure 1.1: Photograph of the Soufrière Hills Volcano, Montserrat, showing the talus slope surrounding the lava dome.

of geologists examining the volcano with an array of ingenious sophisticated apparatus. But these observation are only able to infer what is occurring deep on the inside of the lava dome. Computer models are a safe way[1] to obtain an insight into the internal dynamics of the volcano.

To produce a mathematical model of the internal workings of a volcano some knowledge of the fluid dynamics of lava must be known. Experimentation is not easy as lava cannot be produced in the laboratory, nor can it be collected and manipulated as it tends to melt or ignite what ever it comes into contact with. However, historical experiments with analogous fluids have given an insight into the behavior exhibited by lava.

The term Rheology was coined by Eugene Bingham in 1920 and is the study of stress induced flow in materials, which is now a sub-branch of fluid dynamics and is generally regarded as the study of non-Newtonian fluids. Normal fluids, like water, are categorised as Newtonian fluids and have a fixed viscosity. A non-Newtonian fluid's viscosity is a function of the strain rate

[1] Neglecting mouse induced repetitive strain injuries to the wrist.

applied to the fluid, there are thus two types: shear-thinning and shear-thickening. Lava, along

1.3 Description of this Document

In this dissertation two models of a lava dome volcano and talus slope were developed. Both are height averaged and use a variable Lagrangian mesh to track the expansion of the lava dome. A slab model was produced first as a proof of concept and simplifies the volcano to a cross sectional slab, removing the axi-symmetry of the true system. The radial model was then developed. The models were written in object orientated C++ code.

Chapter 2 derives the equations needed for the Lagrangian cells in the slab geometry and then explains the algorithm used to evolve the system in time. Then Chapter 3 repeats the procedure for the axi-symmetric model explaining all of the differences induced by the change of geometry to the equations and the algorithm. Chapter 4 explains how the models were run and related to the geological observables while Chapter 5 presents all of the results, observations and conclusions as well as making suggestions about how to improve the radial model. In the final Chapter, the conclusions are summarised and ideas for further future work are presented.

Chapter 2

The Slab Volcano

The Rheological approach of [3] which this mathematical model is based on, was developed for

2.1 The Mathematical Model

2.1.1 Rheology Equations

From the paper by Balmforth *et al.* [3], the axi-symmetric rheology equations are rewritten in a one-dimensional slab form;

$$\frac{\partial h}{\partial t} + \frac{\partial U}{\partial x} = w_s(x), \tag{2.1}$$

where $w_s(x)$ is the source term for the lava extrusion as a function of the x co-ordinate, h is the height of the lava dome, and $\frac{\partial U}{\partial x}$ is the change of the rheology term U of the lava with x. The rheology term

$$U = \frac{-n}{n+1}\left|\frac{\partial h}{\partial x}\right|^{\frac{1}{n}-1} Y^{1+\frac{1}{n}}\left[h - \frac{nY}{2n+1}\right]\frac{\partial h}{\partial x}\,\Theta(Y). \tag{2.2}$$

is taken from the paper, where n is an integer which defines the non-Newtonian nature of the lava fluid; $n = 1$ is a pure Newtonian fluid, $n < 1$ is a shear thinning fluid, and $n > 1$ is a shear thickening fluid. $\Theta(Y)$ is the heavyside function with respect to Y,

$$\Theta(Y) = \begin{cases} 0 & Y \le 0 \\ 1 & Y > 0 \end{cases},$$

where Y is defined to be

$$Y = h - \left|\frac{B}{\frac{\partial h}{\partial x}}\right|,$$

and B is the Bingham number of the lava, defined by

$$B = \frac{\tau_p H}{\eta V} = \frac{\tau_p L}{\rho g H^2}.$$

Substituting for $h(I, t)$ gives

$$V_T(t) = \frac{1}{2}(x_T(t) - x_I(t))^2 \tan\theta, \tag{2.5}$$

and rearranging produces

$$x_T = \sqrt{\frac{2V_T}{\tan\theta}} + x_I.$$

say. Equations (2.8) and (2.9) are combined into

$$c_i = \int_{x_{i-1}(t)}^{x_i(t)} \frac{h(x,t)}{V_D(t)}\, dx. \tag{2.10}$$

Since c_i is independent of time, $\dot{c}_i = 0$, hence

$$\frac{d}{dt} \int_{x_{i-1}(t)}^{x_i(t)} \frac{h(x,t)}{V_D(t)}\, dx = 0.$$

Using the chain rule for total derivatives,

$$\frac{dA}{dt} = \frac{\partial A}{\partial t} + \frac{\partial A}{\partial x}\frac{\partial x}{\partial t},$$

gives

$$\frac{\partial}{\partial t} \int_{x_{i-1}(t)}^{x_i(t)} \frac{h(x,t)}{V_D(t)}\, dx + \int \frac{\partial}{\partial x_i} \int_{x_{i-1}(t)}^{x_i(t)} \frac{h(x,t)}{V_D(t)}\, dx \int \frac{\partial x_i}{\partial t} = 0,$$

and via integration of the second term

$$\int_{x_{i-1}(t)}^{x_i(t)} \frac{\partial}{\partial t} \int \frac{h(x,t)}{V_D(t)} \int dx + \int \frac{h(x,t)}{V_D(t)} \frac{\partial x}{\partial t} \int_{x_{i-1}}^{x_i} = 0,$$

which is

$$\int_{x_{i-1}(t)}^{x_i(t)} \frac{\partial}{\partial t} \int \frac{h}{V_D} \int dx + \frac{1}{V_D} \int_{x_{i-1}(t)}^{x_i(t)} \frac{\partial (h\dot{x})}{\partial x}\, dx = 0,$$

where the partial derivative $\frac{\partial x}{\partial t}$ is now written as $\dot{x}_i$ since the cell boundaries are only functions of time. By the quotient rule

$$\int_{x_{i-1}(t)}^{x_i(t)} \frac{V_D h_t - h\dot{V}_D}{V_D^2}\, dx + \frac{1}{V_D} \int_{x_{i-1}(t)}^{x_i(t)} \frac{\partial (h\dot{x})}{\partial x}\, dx = 0,$$

and multiplying by V_D

$$\int_{x_{i-1}(t)}^{x_i(t)} \left[h_t - \frac{h\dot{V}_D}{V_D} + \frac{\partial (h\dot{x})}{\partial x} \right] dx = 0.$$

Substituting from equation (2.1) for h_t and equation (2.10) for c_i gives

$$-\dot{V}_D c_i + \int_{x_{i-1}(t)}^{x_i(t)} \left[w_s(x) - \frac{\partial U}{\partial x} + \frac{\partial (h\dot{x})}{\partial x} \right] dx = 0.$$

Integrating, we get

$$-\dot{V}_D c_i + \int_{x_{i-1}(t)}^{x_i(t)} w_s(x)\, dx - U_i + U_{i-1} + h_i\dot{x}_i - h_{i-1}\dot{x}_{i-1} = 0,$$

but this can be summed for all prevTd[(V1.955T96.2012AwTf5g3d[(D)(V1.95,27(tegriv9625Tf7.2831.793

where $\dot{x}_i$, the rate of change of the i^{th} cell boundary, are the i unknowns to be found for $i = 1, 2 \ldots I$. Also, combining equations (2.3) and (2.7) gives

$$\dot{V}_D = \int_0^{x_c} w_s(x)\, dx - \tan\theta\, (x_T - x_I)(\dot{x}_T - \dot{x}_I),$$

which is inserted into equation (2.12) to yield

$$C_i \tan\theta\, (x_T - x_I)(\dot{x}_T - \dot{x}_I) - C_i \int_0^{x_c} w_s(x)\, dx + \int_0^{x_i(t)} w_s(x)\, dx - U_i + h_i \dot{x}_i = 0. \qquad (2.13)$$

Notice here that the interval of existence for the extrusion function is

$$w_s(x) \qquad [0, x_c],$$

since material is only extruded from the conduit, thus

$$\int_0^{x_i} w_s(x)\, dx = \int_0^{x_c} w_s(x)\, dx \qquad x_i \geq x_c. \qquad (2.14)$$

Notice also that

$$C_I = \sum_{j=0}^{I} \frac{V_j}{V_D} = \frac{V_D}{V_D} = 1,$$

which together with equation (2.14) produces three distinct cases: $x_i < x_c$, $x_i > x_c$, and $x_i = x_I$. Equation (2.13) is now valid only for the case where $x_i < x_c$. In the $x_i > x_c$ case we obtain

$$C_i \tan\theta\, (x_T - x_I)(\dot{x}_T - \dot{x}_I) + (1 - C_i) \int_0^{x_c} w_s(x)\, dx - U_i + h_i \dot{x}_i = 0. \qquad (2.15)$$

In the $x_i = x_I$ case $C_I = 1$ causing cancellation of the extrusion term

$$\tan\theta\, (x_T - x_I)(\dot{x}_T - \dot{x}_I) - U_I + h_I \dot{x}_I = 0,$$

and since h_l

3. Discretise the dome into Lagrangian cells, finding: x_i; h_i; V_i; c_i; C_i i.

4. The extrusion function $w_s(x)$ is chosen from geological observations.

5. Use a di□erence method to estimate the height gradient, $(h_i)_x$ i.

6. Calculate the Rheology term, U_i and its derivative $(U_I)_x$ i via a di□erence scheme.

Once the system is set up the time evolution can begin:

1. Find the cell boundary rates, $\dot{x}_i$ i.

2. Calculate the new cell edges for the time step, x_i using an IVP method.

3. Given the new interface boundary position, iterate the relative dome and talus volume growth until the interface condition for $(h_I)_x$ is satisfied and thus calculate the new talus end position.

4. With the volume of the talus found via iteration, calculate the interface height, h_I.

5. Use back recursion to calculate all of the remaining dome heights, h_i, from h_I.

6. Find the new values of $(h_i)_x$; U_i; $(U_i)_x$.

7. Move to the next time step.

This algorithm is implemented into an object orientated frame work using C++.

2.3 Setting Up The System

2.3.1 The Dome and Talus Geometry

Geological observations show that: the volcanic talus slope is at a constant angle, θ, to the horizontal, and is fixed regardless of the volcano's size; there is a smooth transition between

the talus and the dome, i.e. h and h_x are continuous; when the dome is small it is roughly hemispherical. The initial function of dome height $h(x, 0)$ is therefore taken to be a circle, thus

$$h(x, 0) = \sqrt{h_0^2 - x^2}, \tag{2.23}$$

where h_0 is an initial central maximum dome height at $x = 0$ given from observation; it is acting in this case as the radius of the hemispherical dome. The interface point, x_I, is determined from the geometry of the model to be the point at which the tangent to the dome forms an angle θ to the x axis; thus, from the above

$$h^2 = h_0^2 - x^2.$$

Differentiating implicitly gives

$$2h\frac{dh}{dx} = -2x,$$

so that

$$\frac{dh}{dx} = \frac{-x}{\sqrt{(h_0^2 - x_I^2)}}.$$

At the interface the gradient is equal to the talus slope, $-\tan\theta$, therefore

$$\tan\theta = \frac{x_I}{\sqrt{(h_0^2 - x_I^2)}}.$$

Rearranging gives

$$x_I = \sqrt{\frac{h_0 \tan\theta}{1 + \tan^2\theta}}, \tag{2.24}$$

is h_0; the dome region is constrained by the points $(0,0)$, $(0,h_0)$, (x_l,h_l) and $(x_l,0)$; construct a radius from $(0,0)$ to (x_l,h_l) splitting the dome into two sections; a triangle, constrained by the points $(0,0)$, $(x_l,0)$ and (x_l,h_l); and a 'slice of pie', constrained by the points $(0,0)$, $(0,h_0)$ and (x_l,h_l). The triangle's area is given by $\frac{1}{2}h_l x_l$, while the slice of pie has an area given by $\frac{\varphi}{2}h_0^2$, where φ is some angle between the two radii $(0,0)$, $(0,h_0)$ and $(0,0)$, (x_l,h_l), which needs to be determined. Consider now the talus slope which is the tangent to the circle at the point (x_l,h_l), which is, by definition, perpendicular to the radii $(0,0)$, (x_l,h_l). Then by elementary geometry $\varphi=\theta$ the angle of the talus slope to the horizontal, therefore,

$$V_D(t_0) = \frac{1}{2}\left[h_l x_l + \theta h_0^2\right]. \tag{2.25}$$

Recalling that associated to each cell there is a constant normalized volume, c_i, and a sum of the normalized volumes, C_i, given by equations (2.9) and (2.11), respectively; these must also be determined and are done so as follows. From (2.9) and (2.11)

$$C_i = \sum_{j=1}^{i}\frac{V_j}{V_D}, \tag{2.26}$$

where the sum of all the cell volumes upto i needs to be determined and can be done so by the same method that $V_D(0)$ was in equation (2.25). However, it is not possible to use $\varphi = \theta$ here since, the new region's boundary point (x_i,h_i) is not the location of the talus tangent to the curve $h(x)$. Instead φ is determined through geometry to be

$$\varphi = \tan^{-1}\left[\frac{x_i}{h_i}\right], \tag{2.27}$$

thus, from equations (2.25-2.27) the following expression is obtained for the sum of normalised cell volumes upto i,

$$C_i = \sum_{j=1}^{i} c_j = \frac{1}{2V_D}\left[h_0^2\tan^{-1}\left[\frac{x_i}{h_i}\right] + h_i x_i\right].$$

If the C_i are calculated sequentially for increasing i then the individual cell normalised volumes, c_i can be calculated using

$$c_i = C_i - C_{i-1},$$

which completes the discretisation of the volcanic dome into Lagrangian cells at $t = 0$.

2.3.3 The Extrusion Function

Material is extruded from the conduit deep inside the volcanic dome. The conduit edge is at some distance x_c from $x = 0$, which is estimated from geological observations shortly after a major collapse of the volcanic dome and talus; this essentially wipes the crater floor clean exposing the volcanic conduit momentarily. What the exact form of $w_s(x)$ is inside the vent is relatively unknown, but the simplest form that it could take would be a constant step function,

$$w_s(x) = \begin{cases} w_s & x \le x_c \\ 0 & x > x_c \end{cases}, \tag{2.28}$$

as clearly material is only emitted from inside the conduit. $w_s(x)$ is a vertical velocity distribution such that $\int_0^{x_c} w_s(x)\,dx$ is the total extruded volume rate $\dot{V}_E$. The approximation to a flat velocity distribution is seen to be reasonable from studies of bubble shapes in pyroclastic volcanic pumice [2]; pumice is solidified lava with internal bubbles. Usually bubbles are spherical, however when the lava is emitted close to the conduit walls there is a very high velocity gradient which forms long thin stretched bubbles. This is evidence for a viscosity-driven sigmoid velocity distribution near the conduit edge rather than a step; the step function is used for simplicity. Thus the integral can be found, giving the total extruded volume rate to be

$$\dot{V}_E = w_s x_c.$$

2.3.4 Rheology and Di□erence Methods

The rheology term *U*

time step δt,

$$x_i = x_i + \dot{x}_i \delta t,$$

where x_i is the new position of the cell boundary.

The problem with the Euler method is that it is not stable nor very accurate. Ideally a better time step method should be used, the Backward di□erentiation scheme with a Runge-Kutta predicting the initial points, would be superior. This will produce an unconditionally stable, accurate implicit time step method. However, Newtons method will need to be used to predict the root of the implicit equation.

2.4.2 Finding h_i Using Back-Recursion

The procedure to find the time-evolved dome heights for each Lagrangian cell is actually used after the talus/dome volume balance iteration presented below, but for this iteration to work the penultimate cell height h_{I-1} needs to be found by the back recursion formula which is be presented here.

The Lagrangian normalized cell volume c_i is defined to be a constant and is given by an integral in equation (2.10). The approximation of this integral using the trapezium rule is

$$c_i \approx \frac{(h_{i-1} + h_i)(x_i - x_{i-1})}{2V_D(t)},$$

rearranging for h_{i-1} yields

$$h_{i-1} = \frac{2c_i V_D(t)}{x_i - x_{i-1}} - h_i \tag{2.31}$$

which is a backward recursive formula to obtain all of the h_i given the height at the interface, h_I. The interface height is found using equation (2.33), for the iterated talus volume, as described below.

2.4.3 Talus/Dome Volume Balance Iteration

Equation (2.3) is the conservation law which tells us that the lava extruded in one time step is

thinned to the correct degree to allow the derivative condition to be satisfied; $(h_l)_x$ will be shallower than required.

Conversely, consider a 100% increase in the dome volume so that the talus volume remains unchanged. If the talus volume is unchanged then the interface height will also be unchanged. Even though the cell edges will have moved to increase the width of the cells, the volume of the cell will also increase to match the dome's volume change, and thus the h_{l-1} will have to increase substantially. Since h_l has not changed then $(h_l)_x$ will now be steeper than it was previously, which is incorrect. It is clear that the correct gradient will occur somewhere between

2.4.4 Time Step Results

Once the iterative method has found the dome and talus volumes, h_l is calculated from equation (2.33) and the cell heights h_i are then found back recursively by equation (2.31). The important parameters of the model are the cell boundaries and the cell heights, so they are stored. $(h_i)_x$ is calculated from the difference method given in equation (2.29), which is then used to calculate the lava rheology term U_i using equation (2.2). The left handed difference in equation (2.30) is used to find $(U_l)_x$. Thus, all of the new values for the time step have been found and it is possible to move onto the next one.

Chapter 3

The Radial Volcano System

Now that the slab system has been derived and understood it is possible to move onto the more realistic axi-symmetric model, which correctly represents the cone geometry of a lava dome volcano. The derivation follows a similar rout but there are added complications due to the

and

$$Y$$

$$
\begin{aligned}
&= 2\pi \tan\theta \int_{r_I}^{r_T} (r_T r - r^2)\, dr, \\
&= 2\pi \tan\theta \left[\frac{r_T r^2}{2} - \frac{r^3}{3} \right]_{r_I}^{r_T} \\
&= \frac{\pi}{3} \tan\theta \left(r_T^3 - 3 r_T r_I^2 + 2 r_I^3 \right). \qquad (3.3)
\end{aligned}
$$

The talus volume rate is found by implicit differentiation with respect to time, since r_T and r_I are both functions of time;

$$\dot{V}_T = \pi \tan\theta \left(r_T^2 \dot{r}_T - 2 r_T r_I \dot{r}_I - \dot{r}_T r_I^2 + 2 r_I^2 \dot{r}_I \right). \qquad (3.4)$$

Similarly the initial volume of the dome, which is bounded by the arc of a circle, needs to be found via

$$V_D$$

3.1.3 Lagrangian Mesh

Consider now the constant normalised volume Lagrangian cells, such that the rate of change of c_i with time is zero as before. As with the slab model it is possible to sum all of the cells upto i, therefore we can take

$$dC_i$$

where $\frac{\partial r_i}{\partial t}$ is rewritten as $\dot{r}_i$. Use of the quotient rule on the first term and then multiplying through by V_D results in

$$2\pi \int_0^{r_i} \left[rh_t - \frac{rh\dot{V}_D}{V_D} \right] dr + 2\pi\, h_i r_i\, \dot{r}_i = 0.$$

Equation (3.1) and the integral form of C_i are substituted for the first and second terms, respectively, giving

$$2\pi \int_0^{r_i} \left[rw_s(r) - \frac{\partial}{\partial r}(rU) \right] dr + 2\pi\, h_i r_i\, \dot{r}_i = C_i \dot{V}_D.$$

and then performing the integration

$$\pi w_s r_i^2 - 2\pi U_i r_i + 2\pi\, h_i r_i\, \dot{r}_i = C_i \dot{V}_D,$$

which gives i equations for the i unknowns $\dot{r}_i$. Equation (3.2) is substituted for $\dot{V}_D$, the unknown rate of change of dome volume,

$$\pi w_s r_i^2 - 2\pi U_i r_i + 2\pi\, h_i r_i\, \dot{r}_i = C_i \pi w_s r_c^2 - C_i \dot{V}_T. \tag{3.7}$$

Since $\dot{V}_T$, the rate of change of talus volume, is given by equation (3.4) we realise here that each of the i equations also contains the unknowns $\dot{r}_I$ and $\dot{r}_T$, which can be removed as follows.

3.1.4 Formation of the Last Equation

Consider $\dot{r}_T$: The rate of change of the interface height due to the talus is given by equation(2.17) (with $x \to r$), which rearranges to give

$$\dot{r}_T = \frac{1}{\tan\theta} \frac{\partial h_I}{\partial t} + \dot{r}_I.$$

However, $\frac{\partial h_I}{\partial t}$ is not known, though differentiating equation (3.1) by the product rule allows it to be eliminated, together with the observation that $w_s(r_I) = 0$, this yields

$$\frac{\partial h_I}{\partial t} + \frac{U_I}{r_I} + \frac{\partial U_I}{\partial r} = 0,$$

therefore

$$\dot{r}_T = \dot{r}_I - \frac{1}{\tan\theta}\left[\frac{U_I}{r_I} + \frac{\partial U_I}{\partial r}\right]. \tag{3.8}$$

Now consider $\dot{r}_I$: If we recall that for the I^{th} equation in (3.7)

3.1.5 Equations as a Matrix System

The i equations in i unknowns given in equation (3.7) form the matrix system

$$\mathrm{K}\underline{r} = \underline{f},$$

where K is an $I \times I$ matrix

$$\mathrm{K} = \begin{bmatrix} K_1 & 0 & 0 & 0 & M_1 \\ 0 & K_2 & 0 & 0 & M_2 \\ 0 & 0 & \ddots & \vdots & \vdots \\ 0 & 0 & \cdots & K_{I-1} & M_{I-1} \\ 0 & 0 & \cdots & 0 & M_I \end{bmatrix},$$

and $\underline{r}$ and $\underline{f}$ are the vectors

$$\underline{r} = \begin{bmatrix} r_1 \\ r_2 \\ \vdots \\ r_I \end{bmatrix} \quad \text{and} \quad \underline{f} = \begin{bmatrix} f_1 \\ f_2 \\ \vdots \\ f_I \end{bmatrix}.$$

The system can be rewritten

$$\mathrm{D}\,\underline{r} + \mathrm{M}\underline{r} = \underline{f},$$

where D is a diagonal matrix and the denoted a size of $(I - 1)$ and

$$\mathrm{M} = \begin{bmatrix} 0 & 0 & 0 & 0 & M_1 \\ 0 & 0 & 0 & 0 & M_2 \\ 0 & 0 & \ddots & \vdots & \vdots \\ 0 & 0 & \cdots & 0 & M_{I-1} \\ 0 & 0 & \cdots & 0 & M_I \end{bmatrix}.$$

Thus

$$\mathrm{D}\,\underline{r} + r_I \underline{m} = \underline{f},$$

where $\underline{m}$ is now a column vector. The I^{th} equation is now simply

$$r_I M_I = f_I,$$

thus the matrix system

$$\mathrm{D}\,\underline{r} = \underline{f} - \frac{f_I}{M_I}\underline{m}$$

can now be solved. From equation (3.7) and (3.10) we can identify

$$\begin{aligned}
K_i &= 2h_i r_i, \\
M_i &= C_i \tan\theta (r_T - r_I)^2, \\
M_I &= \tan\theta (r_T - r_I)^2 - 2h_I r_I, \\
f_i &= C_i w_c r_i^2 + 2U_i r_i - w_i r_i^2 + C_i \left[r_T^2 - r_I^2 \left[\frac{U_I}{r_I} + \frac{\partial U_I}{\partial r} \right] \right], \\
f_I &= 2U_I r_I + \left[r_T^2 - r_I^2 \left[\frac{U_I}{r_I} + \frac{\partial U_I}{\partial r} \right] \right]
\end{aligned}$$

noticing that the factor of π has cancelled.

3.2 The Algorithm

Equations (3.7) and (3.11) provide a way to find the rates of change of the Lagrangian cell boundaries in the radial geometry; however, as before what is really required is the evolution of the dome height and growth of the talus slope with time. The algorithmic method to find these is similar to the one given for the slab model and is given briefly here;

Set up the system at $t = 0$:

1. Chose an initial height distribution for the dome and talus, $h(r, 0)$, from geological ob-

servations.

2. Given the interface condition for $(h_I)_r$ and the initial function $h(r, 0)$, find the talus end point r_T, the interface location, r_I and the total dome volume, V_D.

3. Discretise the dome into Lagrangian cells, finding: r_i; h_i; V_i; c_i; C_i i.

4. Use a difference method to estimate the height gradient, $(h_i)_r$ i.

5. Calculate the Rheology term, U_i and its derivative $(U_I)_r$ i via a difference scheme.

Once the system is set up the time evolution can begin:

1. Find the interface boundary rate $\dot{r}_I$ and us it to calculate the talus volume rate, $\dot{V}_T$.

2. Find the remaining cell boundary rates, $\dot{r}_i$ for $i = 1, 2...(I - 1)$.

3. Calculate the new cell edges for the time step, x_i using an IVP method.

4. Given the new interface boundary position, iterate the relative dome and talus volume growth until the interface condition for $(h_I)_x$ is satisfied

5. Calculate the new talus end position from the new talus volume using Newtons method.

6. Calculate the interface height, h_I from the talus end position.

7. Use back recursion to calculate all of the remaining dome heights, h_i, from h_I.

8. Find the new values of $(h_i)_x$, U_i, and $(U_i)_x$.

9. Move to the next time step.

3.3 Setting Up The Radial System

3.3.1 The Dome and Talus Geometry

The method of setting up the initial dome and talus geometry is identical to the one presented in Section 2.3.1 for the slab geometry (with x replaced by r), since it is simply based on the cross sectional geometry through the volcano from $r = 0$ to $r = r_T$.

3.4 Time Step Evolution of the System

3.4.1 Lagrangian Cell Boundaries

When the radial volcanic system has been initialised then the rate of change of the talus/dome interface with time can be found from equation (3.11), which is used to calculate the rate of change of the talus volume from equation (3.9). This allows all of the remaining cell boundary rates of change to be found from equation (3.7). The Euler method is used to find the new cell boundaries from the rates in the same way as it was for the slab model.

3.4.2 Talus/Dome Volume Balance Iteration

The bi-section iteration for the dome and talus volumes using the interface condition $(h_I)_r = -\tan\theta$ as a constraint runs exactly as laid out in Section 2.4.3. However, here the equation for the rate of change of the volume of the talus is now given by (3.4) which is a cubic polynomial in r_T, the end of the talus slope. Calculation of r_T for each iteration of the bi-section method is not possible directly, as it was for the slab model; Newton's method must be used. The cubic polynomial in r_T is

$$f(r_T) = r_T^3 - 3r_I^2 r_T + 2r_I^3 - \frac{3V_T}{\pi \tan\theta}.$$

Newton's method to find the primary root of $f(r_T)$ is

$$r_{n+1} = r_n - \frac{f(r_n)}{f'(r_n)}, \tag{3.13}$$

where $f'(r_T)$ is the differential of $f(r_T)$,

$$f'(r_T) = 3r_T^2 - 3r_I^2,$$

3.4.4 Time Step Results

Once the iterative method has found the dome and talus volumes, all of the h_i are calculated from the back recursion equations. The important parameters of the model are the cell boundaries and the cell heights, so they are stored. $(h_i)_r$, U_i and $(U_i)_r$ are calculated from difference methods and thus, all of the new values for the time step have been found and it is possible to move onto the next one.

Chapter 4

Running the Models

Once the models have been translated into object orientated computer code they can be run to generate results for the evolution of the slab and radial volcanic dome and talus systems. It is not a case of simply inserting the parameters observed by geologists, presented below, into the models to obtain meaningful results. Non-dimensionalisation of the system must be used and will be discussed below, before moving on to present the specifics of running the models. Results and subsequent discussions are then presented in the next Chapter.

4.1 Geological Observations of The Volcanic system

Geological observations [10] of a typical lava dome volcano on the island of Montserrat were made between 15^{th} November 2005 and 20^{th} May 2006, which correspond to days 3642 - 3839 measured from the beginning of lava extrusions ten years previously. The observations are:

- The gradient of Talus remains constant at approximately 35^{o}. The slope is 37^{o} on the uppermost parts and 32^{o} on the lowermost.
- After a major dome collapse event the volcanic conduit can be seen on the crater floor, it is estimated to be 30 meters in diameter.
- The volume of the entire volcano was estimated approximately once a month and from

that the volume of material extruded was calculated. The extruded volume rate is seen to be dynamic over the six months of observations; an average estimate is $\dot{V}_E = 6\text{m}^3/\text{s}$.

- Measured from the crater floor, h_0, the dome's central maximum height grew from 55 meters to 326 meters between the above dates.
- At the end of the measurement period the talus slope was 930 meters from the centre of the conduit, r_T.

4.2 Non-dimensionalisation

Non-dimensionalisation is the process of removing units from a system of mathematical equations by substitution of variables. The essence of this process is to obtain a system where all variables are less than unity and are all approximately the same size, which releases the dynamic dependence of terms with one another as the model evolves rather than the possible situation where one term dominates the evolution and thus the results. The recipe used here is described in detail in [3] but is summarised here for clarity.

The characteristic horizontal and vertical lengths, H and L, are chosen to represent the volcanic system. From these a characteristic horizontal velocity, V is chosen to be

$$V = \frac{\rho g H^3}{\eta L},$$

where ρ is the lava density, g is the acceleration due to gravity and η is the lava's viscosity. The new system variables (represented by the tildes) are as follows:

$$\tilde{r} = \frac{r}{L}, \qquad \tilde{h} = \frac{h}{H}, \qquad \tilde{w} = \frac{wL}{VH}, \tag{4.1}$$

where w is a vertical velocity, i.e. the extrusion velocity of the lava, w_s.

The paper then derives the Bingham number of the lava fluid to be

$$B = \frac{\tau_p H}{\eta V} = \frac{\tau_p L}{\rho g H^2},$$

where τ_p is the yield stress of the fluid. Values of the variables are given to be

$$\tau_p = 10^5 \text{Pa}, \qquad \rho = 2600 \text{kg m}^{-3}, \qquad \eta = 10^9 \text{Pa s},$$

with $g = 10 \text{m s}^{-1}$ as usual.

To perform the non-dimensionalisation in this case, L and H need to be chosen. Starting with the information that at the beginning of the observation period the maximum height of the dome was 55 meters, and using the dome/talus set up procedure described in Section 2.3.1 the end of the talus is found to be 95 meters. The characteristic dimensions are taken to be ten times larger than these parameters; $L = 950$ and $H = 550$ to force the requirement that $\tilde{r}$ and $\tilde{h}$ be smaller than unity, while allowing large growth before reaching the characteristic values. The rest of the values are as follows:

$$\tilde{r} = 0.1, \qquad \tilde{h} = 0.1, \qquad V = 4.55 \text{m/s}, \qquad B = 0.01.$$

$\tilde{w_s}$, is found from the volume extrusion rate given by the geological observations. The velocity will not be the same for the slab and radial models due to the different geometry. For the slab system $\dot{V}_E = 2x_c w_s$ thus, $w_s = 0.2 \text{m/s}$ and $\tilde{w_s} = 0.076$. While for the radial system $\dot{V}_E = \pi w_s r_c^2$, thus $w_s = 0.0085 \text{m/s}$ and $\tilde{w_s} = 0.0032$.

There also exists a characteristic time, $T = \frac{L}{V}$ which gives a non-dimensional unit of time as

$$\tilde{t} = \frac{t}{T} = 0.005. \tag{4.2}$$

4.3 The Slab Model - Choosing δt and I

Initially it is very difficult to choose a good time step size, δt, and number of Lagrangian cells, I, that will allow an accurate stable evolution of the volcanic system, due to the complex nature of the model. The initial time step size was chosen to be the non-dimensional time found above, since this is the natural unit of time for the system; the number of cells chosen was 30. The code was run repeatedly with various time steps and cell number to observe the models behavior. The model was deemed to run successfully if it reached one million time steps without failing and did not have appreciable oscillations in the final solution of the height.

Model	I	δt	N_{steps}	Comment/failure
A	30	0.005	40903	Convergence - oscillations
B	30	0.01	0	Convergence failure
C	30	0.0025	66465	Convergence - oscillations
D	30	0.001	125163	Convergence - oscillations/-ve(52-694)
E	30	0.0005	201228	Convergence - oscillations/-ve(131-323)
F	30	0.00025	322592	Convergence - oscillations/-ve(37-1870)
G	30	0.0001	600338	Convergence - oscillations/-ve(32-3515)
H	30	0.00005	958726	Convergence - oscillations/-ve(30-0d90m0.1139nen8726

recovered from it and a discontinuity in the gradient at the interface was seen to grow. For this reason the first failure of the bi-section algorithm was taken as the ultimate point of failure of the model. However, studies suggest that there are two underlining reasons for the convergence failure: either growth of oscillations in the height; or negative cell boundary velocities; see Section 5.1.

Figure 4.1 shows the input parameters of several models which were run and their outcome. From the starting value of δt in model A, the time step was then increased in size to 0.01 and the model failed on the first iteration, this would appear to be a good estimate of the maximum time step allowed for the system to remain stable for several iterations. From here the time step is reduced until a successful outcome is achieved in model J. Subsequent models had their number of cells increased, the time step was seen to require further reduction to again obtain a long lasting stable solution.

4.4 The Radial Model - Choosing δt and l

Theoretically, the radial model is a more realistic representation of reality than the slab model, as already discussed, because it reproduces the axi-symmetric geometry of a real volcano.

Model	I	δt	N_{steps}	Comment/failure
A1	30	0.005	0	Total convergence failure
B1	30	0.0025	24	Convergence -ve $\dot{x}_i$
C1	30	0.001	60	Convergence -ve $\dot{x}_i$
D1	30	0.0005	86	Convergence -ve $\dot{x}_i$
E1	30	0.00025	104	Convergence -ve $\dot{x}_i$
F1	30	0.0001	116	Convergence -ve $\dot{x}_i$
G1	30	0.00005	121	Convergence -ve $\dot{x}_i$
H1	30	0.000025	123	Convergence -ve $\dot{x}_i$
J1	30	0.00001	125	Convergence -ve $\dot{x}_i$
K1	30	0.000005	125	Convergence -ve $\dot{x}_i$
A2	40	0.005	0	Total convergence failure
B2	40	0.0025	16	Convergence -ve $\dot{x}_i$
C2	40	0.001	56	Convergence -ve $\dot{x}_i$
D2	40	0.0005	76	Convergence -ve $\dot{x}_i$
E2	40	0.00025	86	Convergence -ve $\dot{x}_i$
F2	40	0.0001	90	Convergence -ve $\dot{x}_i$
G2	40	0.00005	91	Convergence -ve $\dot{x}_i$
H2	40	0.000025	92	Convergence -ve $\dot{x}_i$
A3	50	0.005	0	Total convergence failure
B3	50	0.0025	16	Convergence -ve $\dot{x}_i$
C3	50	0.001	150	Convergence -ve $\dot{x}_i$
D3	50	0.0005	94	Convergence -ve $\dot{x}_i$
E3	50	0.00025	79	Convergence -ve $\dot{x}_i$
F3	50	0.0001	76	Convergence -ve $\dot{x}_i$
G3	50	0.00005	75	Convergence -ve $\dot{x}_i$
A4	20	0.005	0	Total convergence failure
B4	20	0.0025	13	Convergence -ve $\dot{x}_i$
C4	20	0.001	81	Convergence -ve $\dot{x}_i$
D4	20	0.0005	123	Convergence -ve $\dot{x}_i$
E4	20	0.00025	153	Convergence -ve $\dot{x}_i$
F4	20	0.0001	175	Convergence -ve $\dot{x}_i$
G4	20	0.00005	184	Convergence -ve $\dot{x}_i$
H4	20	0.000025	189	Convergence -ve $\dot{x}_i$

Model	I	δt	N_{steps}	Comment/failure
A5	15	0.005	0	Total convergence failure
B5	15	0.0025	9	Convergence -ve $\dot{x}_i$
C5	15	0.001	99	Convergence -ve $\dot{x}_i$
D5	15	0.0005	207	Convergence -ve $\dot{x}_i$
E5	15	0.00025	240	Convergence -ve $\dot{x}_i$
F5	15	0.0001	252	Convergence -ve $\dot{x}_i$
G5	15	0.00005	259	Convergence -ve $\dot{x}_i$
H5	15	0.000025	263	Convergence -ve $\dot{x}_i$
J5	15	0.00001	264	Convergence -ve $\dot{x}_i$

Figure 4.2: Running the radial model failed to find one that was successful and stable.

The first values of δt and I were taken to be the same as they were for the slab model. Then, δt was decreased and I increased in the hope of finding a stable model evolution. None were found; all of the attempts are displayed in Figure 4.2. All of the models exhibited the same behavior: the cells started with positive $\dot{x}_i$ for several iterations; with each consecutive iteration $\dot{x}_i$ decreases until eventually the last one, $\dot{x}_I$, becomes negative; the rest then swiftly follow within a few iterations; eventually the cell boundaries cross over producing negative heights and the model terminates shortly afterwards. No models recovered or ran for long once negative velocities had emerged. Thus, the final number of iterations displayed in Figure 4.2 was the point at which the model developed negative $\dot{x}_i$.

Eventually I∆.955Tf9l1d.lly

Chapter 5

Results and Discussion

5.1 The Slab Model

Of the seventeen versions of the slab model presented in Figure 4.1 three are carefully selected and presented here to demonstrate the main three types of behavior displayed:

Model A is chosen first because it is one of the few that runs without negative values of $\dot{x}_i$ appearing, it also forms height oscillations which are visible after 40000 iterations as shown in Figure 5.1.

Model M is selected because it is one of the few runs which fails while it has negative values of $\dot{x}_i$. It is also unusual that it starts with negative call boundary velocities before moving into a fully positive phase before returning to negative ones again. It quickly develops large oscillations, demonstrated in Figure 5.2, and thus ultimately fails to converge.

Model T is chosen because it was the most stable solution found after running many versions of the code and carefully selecting the input parameters between each run. It was one of only two models which ran to one million iterations but it had smaller oscillations than model J. If the model is run for half a million time steps then there are no oscillations; as displayed in Figure 5.4. However, the volcano has grown so much relative to the original that it is difficult

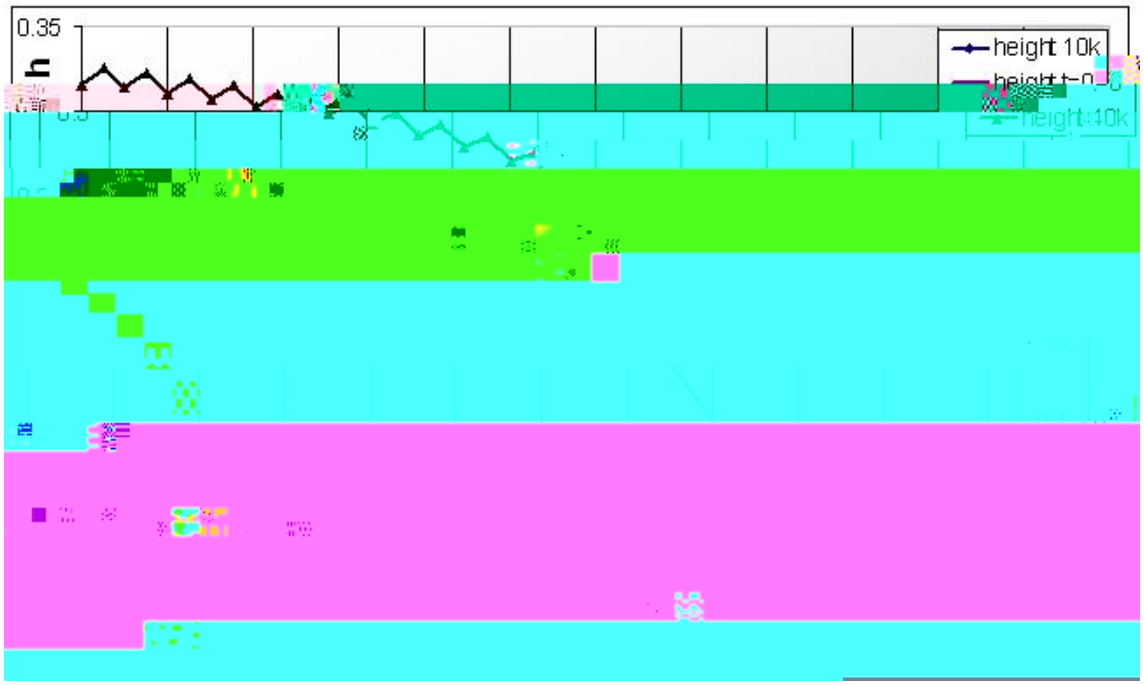

Figure 5.1: Model A - δt = 0.005 I = 30: the initial geometry at t = 0; 10000 iterations; and the termination of the model at 40903 iterations.

to compare the two, for this reason two plots are made using this model, both of which contain the height distribution after 50000 steps, for comparison.

Generally, as the models in Figure 4.1 were run, the time step and cell widths were decreased, this means that the later models will be more stable and accurate; which is why they ran successfully for a greater number of iterations.

Model A (Figure 5.1) did not undergo a period of negative cell velocities and for this reason the evolution of the model rapidly moves horizontally. Between zero and 10000 iterations there is substantial height increases too. However, from 10000 to the termination of the model at a little over 40000 steps it is noticed that beside the growth of oscillations, the height of the interface has grown only very slightly. It is observed that the oscillations in the height start at small x and grow in height, as they grow they also move along the solution to larger x, until eventually they reach the interface and grow further. Ultimately the model fails because the bi-section iteration cannot find a volume fraction for the dome and talus which allows the gradient condition to be satisfied. This model is clearly unstable and will generate a less accurate height

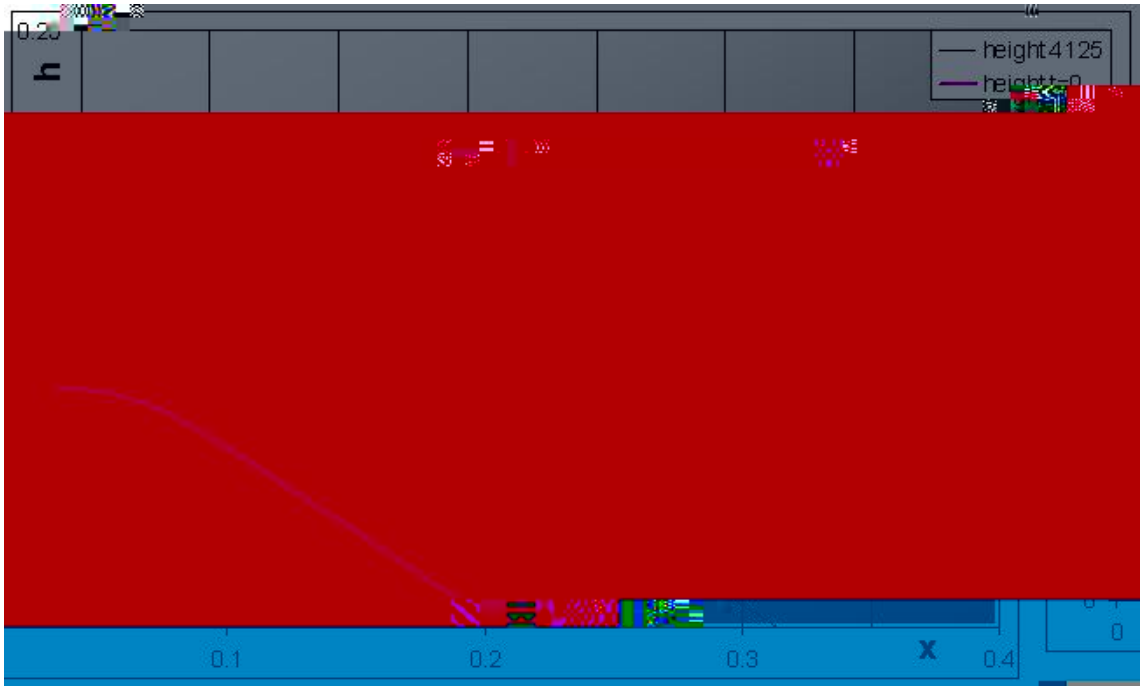

Figure 5.2: Model M- δt = 0.0005 I = 50: the initial geometry at $t = 0$ and the termination of the model at 4125 iterations.

evolution than ones with smaller δt and larger I; it is thus discarded when drawing conclusions relating to reality.

Model M (Figure 5.2) undergoes two periods of negative growth with positive growth for several thousand iterations in between. The first period contains negative $\dot{x}_i$ for the cells nearest to x = 0 and starts with only a few cells, grows upto eight negative cells and then decays back to positive growth, this period appears smooth and well structured. The second period however, displays di□erent characteristics, with alternate cell edges being positive and negative throughout the cell range on one time step and then all positive on the next time step;

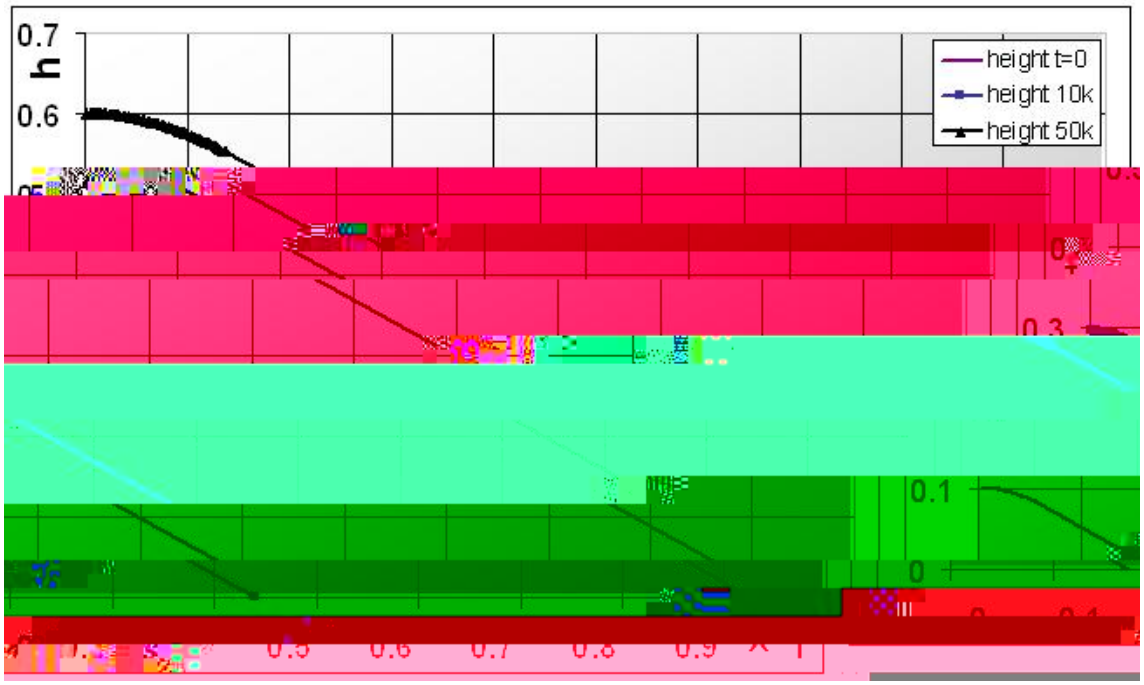

Figure 5.3: Model T- δt = 0.00001 I = 75 :the initial geometry at $t = 0$; 10000 iteratT[(=)natT10T8]Q]T

This model is also discarded as it is unstable.

Model T (Figures 5.3 and 5.4) is stable for half a million iterations and only small oscillations, in the region of 0.1%, developed after a total of one million steps. For this reason it is felt that this is the most accurate model. It is noticed that the first 9816 steps have some negative cell velocities, investigation shows that it is several cells at small x and the number of them swells and decays rhythmically upto a maximum of about twelve cells before eventually returning to an entirely positive state. The plot after the first 10000 steps shows that the talus/dome interface has actually moved to the left but grown in height substantially, it is only after this period that all of the cells acquire positive velocities and the interface moves to the right.

At first this would seem counter intuitive, as surly the volcano must simply grow if material is extruded into it. Well, if we examine equations (2.20-2.22), which are responsible for producing the cell edge velocities, we see that C_i is constant and that the amount of material extruded into a cell will not change by much if the cell width changes only slowly; which it must do as the negative values of $\dot{x}$

Then the dome slows its vertical growth and enters a period dominated by horizontal growth which pushes the talus outward, the talus volume growth slows because $(h_l)_t$ is smaller.

It would be interesting to compare this model with the rate of pyroclastic flows, which form the talus, to see if they decrease as the volcano grows, echoing the slowing of the talus volume increase. However, it may be that the frequency of pyroclastics with certain start locations changes from the top of the dome to lower down the slopes as a function of volcano size, this would occur as the talus is pushed out by the expanding dome and restructuring itself internally rather than having new material distributed onto its surface.

However, it must be realised that the slab model is not entirely physical, as already discussed.

5.2 The Radial Model

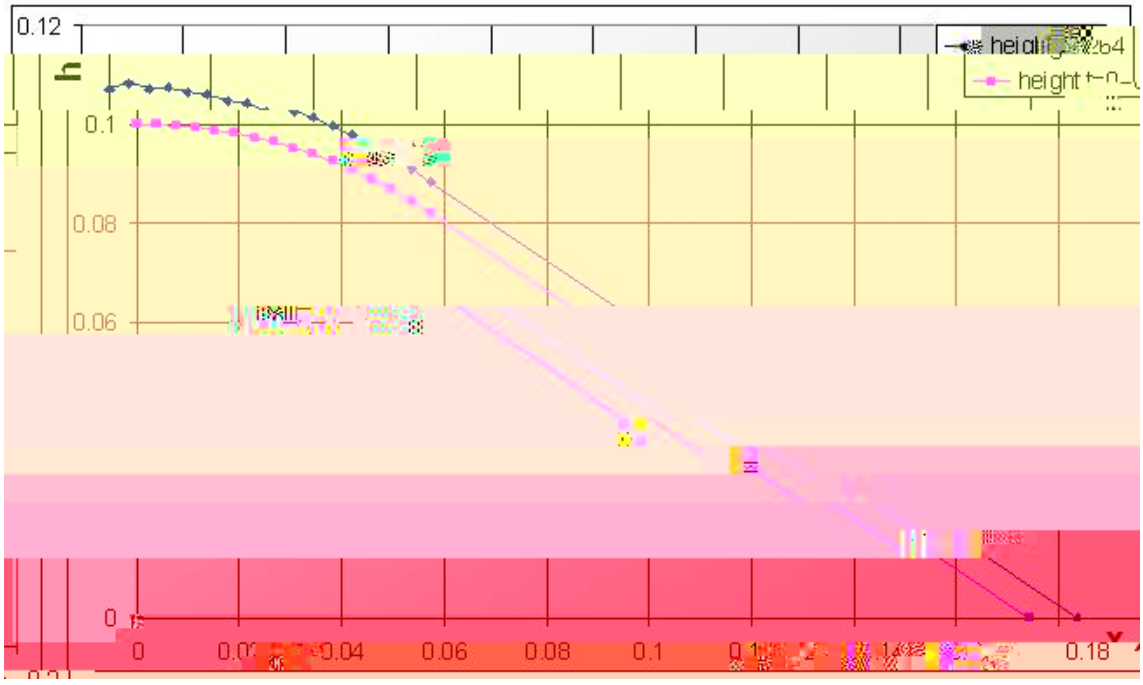

Figure 5.5: Model J5 - δt = 0.00001 I = 15: the initial geometry at t = 0 and after 264 iterations when the model failed.

Figure 5.5 shows the resultant height distribution after the 264 time steps of radial model J5. Even though this model has only had positive cell boundary velocities the cell edges are

seen to have changed little, with the majority of the dome's growth going into the height of the cells. The first sign of oscillations has appeared at small x but they do not get the opportunity to manifest the entire distribution before some $\dot{x}_i$ become negative, which for the radial model is terminal. However, we recall that for the most accurate and stable slab model run (T) there was a period when several cells had $\dot{x}_i < 0$ and this was deemed to be satisfactory behavior. It would thus appear plausible that the radial model should follow a similar path of initial vertical growth followed later by horizontally dominated growth. The radial model would thus appear to be initially producing good results before premature termination.

The observation that the model fails earlier when more cells are included can be explained by the fact that the cell boundary velocities are not dependent on the width of the cell but its upper edges location relative to the origin and the conduit, and via incorporation into U_i, the height and its x derivative. Thus, when there are more cells it takes less time for the boundaries to cross one another, if the time step is not reduced appropriately. However, given the observation that the first appearance of negative velocities stablises to a fixed number of iterations as δt decreases then it is clear that the model will fail sooner when I increases if the time step size is at this limit; as displayed in Figure 4.2.

We conclude that two investigations need to be launched: the first should further examine the causes and behavior of the appearance and growth of negative $\dot{x}_i$ from the interface via comparisons with the slab model; the second should look at the counter intuitive failure of the model to run for more time steps for smaller δt and larger I.

There are some initial criticisms of the way that the radial model is structured which should be improved, however, whether these are the responsible for the failings highlighted above is unclear.

The first is that when the slab model was built the Lagrangian cells were split into equal widths and thus had normalized volumes, c_i, of roughly the same magnitude. In the radial model the x separation of the cell edges has not changed, however, now the volumes are annular rings and thus the volumes are not of similar magnitude. The cell widths should be changed to

obtain volumes of approximately the same size, *i.e.* $\Delta r \quad \frac{1}{r}$. Exactly what effect this feature will have is unclear, but it could well be equivalent to having a variable stability across the dome as the cells change in magnitude; which clearly is not ideal.

The second is that there is a subtle approximation occurring when the bi-section method finds the dome and talus volume rates. The algebra will produce a different value based on terms from the previous time step, which is then used to calculate $\dot{x}_i$. This will be correct to first order but it would be better to implement some form of iterative approach to update values so that the algebraic and iterative volume rates are the same; a suitable method needs to be found. Of cause it could also be that the best way to include the interface gradient condition of $(h_I)_x = -\tan\theta$ is not through an iterative approach, as it may prove possible to include it algebraically, this should also be investigated.

5.3 Re-Dimensionalisation

Once the models have been run it is straight forward to return the system to real units using equations (4.1) and (4.2). Slab model T displayed after 50000 time steps in Figure 5.3 can be calculated to have grown from 55 to 330 meters in height and from 95 to 880 meters in length in a time of 100 seconds; which is substantially faster than the reality displayed in Section 4.1. However, the height is very close but the talus a little short.

5.4 Comparisons With Previous Work

As far as is known this is the first study of lava dome volcano growth to incorporate the talus slope. This means that the results presented here are not directly compatible with the results of previous work. Also, it is ideally the radial model which should be compared with other

Chapter 6

Conclusions and Future Opportunities

6.1 Summary of Conclusions

Two height averaged expanding Lagrangian mesh models were developed of a lava dome volcano and it's attached talus slope; the first used a simple slab geometry while the second was axi-symmetric. The models were developed in C++ using an object orientated class frame-work. The following observations were drawn:

- An accurate and stable solution of the slab model was found with 75 cells and a time step of $\delta t = 0.00001$ which ran for one million iterations.
- No stable solution could be found for the radial model.
- Models which failed did so due to lack of convergence of the bi-section method of obtaining dome/talus volume balance at the interface.
- It was discovered that there were two reasons for this: oscillations in the height distribution; and negative cell boundary velocities.
- Unstable slab models eventually suffered from oscillations in the height distribution, while all radial models eventually suffered from negative cell velocities.

- Oscillations of the height solution in the slab model are believed to arise from the Euler time step method and the trapezium rule estimate of the back recursion height calculation; these need to be improved.

- Features leading to the failure of the radial model need further investigation, though the volume of the Lagrangian cells is suspected as being contributory alo-1(o)1(nl-27((l451(47((

6.2 Future Opportunities

6.2.1 Improvements to the Radial Model

Immediate improvements to the radial model should be:

- Better selection of the Lagrangian cell widths to obtain similar normalized volumes for all cells.
- Replacement of the Euler time step, with a backward differentiation method using a Runge-Kutta to find the first few steps will produce an unconditionally stable time stepping method.
- An improvement of the back recursion via the trapezium rule needs to be found.
- Investigate the appearance and spread of negative cell boundary velocities.
- Improve the implementation of the interface boundary gradient condition.
- Production of a version of the model without the talus.

6.2.2 Improvements to the Talus Representation

In the models presented here, the talus is simply represented by a slope who's size is governed by constrains based on geological observations. the dynamics of what is occurring inside the granular structure of the slope is not included; ideally this should be represented.

There are many studies of talus slope structures [11]-[15], ranging from observational statistical sorting of debris to experiments on sand piles to rigorous Navier-Stokes fluid dynamical models. It would be premature to consider the statistical sorting of rock sizes throughout the talus due to the dynamics of their deposition by descent. The Navier-Stokes approach is a recent competitive model to the well established Savage-Hutter model, [16] and [17], which has invoked great interest in the literature as shown in a recent review [18]. Even though it was originally developed for snow avalanches the Savage-Hutter model would appear to be the most

promising way forward. Briefly summarised, this model consists of the hyperbolic partial differential equations of a depth averaged down-slope velocity u and local avalanche layer thickness h:

$$\frac{\partial h}{\partial t} + \frac{\partial}{\partial t}(hu) = 0; \tag{6.1}$$

$$\frac{\partial}{\partial t}(hu) + \frac{\partial}{\partial t}\left[hu^2 + \frac{\beta_x}{2}h^2 \right] = hs_x; \tag{6.2}$$

where s_x is a dynamic driving force and β_x is a dynamic pressure/friction coefficient. Application of these equations to the talus slope as Lagrangian cells need to be investigated as well as the interaction at the dome/talus interface with the Rheological lava equations. This method should make it possible to obtain an expression for the velocity of the end of the talus slope, which would remove the need for an iterative approach to finding the volume rates of the dome and the talus.

It could also prove feasible to recreate the pyroclastic deposition of material onto the talus as a shock like event by using conservation law schemes [19].

6.2.3 Moving to Two Dimensions

At this stage it is not clear if it is possible to represent the dome and the talus as a two dimensional Lagrangian grid. However, if it is feasible, then this will allow the talus to take on a non-triangular shape as the interface will be able to flex freely, rather than being a vertical line; this would be a better representation of reality.

Ultimately but probably much further into the future it would hopefully be possible to build a full two-dimensional finite element model of the talus slope and add it onto the lava dome models presented in [1] which are currently being developed further [20]. However, due to the nature of the expansion of the volcano, the finite element method will need to incorporate a moving mesh, thus it may well be beneficial to investigate the implementation of the appropriate

talus dynamics within a Lagrangian framework first.

Bibliography

[1] A.J. Hale, *Computationally Modelling the Lava Dome at the Soufriere Hills Volcano, Montserrat*, PhD Thesis. Reading University (2004),

[2] J. Blower, *Bubble Formation in Lava*, PhD Thesis. Bristol University

[3] N.J. Balmforth, A.S. Burbidge, R.V. Craster, J. Salzig & A. Shen *Visco-Plastic Models of Isothermal Lava Domes* J. Fluid Mech. (2000), vol. 403, pp. 37-65

[4] N.J. Balmforth, R.V. Craster & R. Sassi *Dynamics of Cooling Viscoplastic Domes* J. Fluid Mech. (2004), vol. 499, pp. 149-182

[5] R.W. Gri□ths & J.H Fink *Solidifying Bingham Extrusions: A Model for the Growth of Silicic Lava Domes* J. Fluid Mech. (1997), vol. 347, pp. 13-36

[6] D.I. Osmond & R.W. Gri□ths *The Static Shape of Yield Strength Fluids Slowly Emplaced on Slopes* J. Geophys. Res. (2001), vol. 106, pp. 16241-16250

[7] A.J. Hale & G. Wadge *Numerical Modelling of the Growth Dynamics of a Simple Silicic Lava Dome* Geophys. Res. letters (2003), vol. 30, No 19

[8] R.M. Iverson *Lava Domes Modeled as Brittle Shells that Enclose Pressurized Magma, with Application to Mount St. Helens* Journal source unknown

[9] H.E. Huppert, J.B. Shepherd, H. Sigurdsson & R.S.J. Sparks *On Lava Dome Growth with Application to the 1979 Lava Extrusion of the Soufriére of St. Vincent* J. Volc. Geoth. Res. (1982), vol. 14, pp. 199-222

[10] Geo Wadge, Private e-mail communications.

[11] F.L. Perez *Talus Fabric and Particle Morphology on Lassen Peak, California*, Geogr. Ann. (1989), vol. 71A(1-2), pp. 43-57

[12] K. Li man, M. Nguyen, G Metcalf & P Cleary *Forces in Piles of Granular Material: An Analytic and 3D DEM Study*, Granular Matter (2001), vol. 3, pp. 165-176

[13] I. Statham *A Scree Slope Rockfall Model*, Earth Surf. Proc. (1976), vol. 1, pp. 43-62

[14] B. Voight & D. Elsworth *Failure of Volcano Slopes*, Geotechnique (1997), vol. 47(1), pp. 1-31

[15] P. Jop, Y. Forterre & O. Pouliquen *A Constitutive Law for Dense Granular Flows*, Nature (2006), vol. 441, pp. 727-730

[16] S.B. Savage & K. Hutter *The Motion of a Finite Mass of Granular Material Down a Rough Incline*, J. Fluid Mech. (1989), vol. 199, pp. 177

[17] S.B. Savage & K. Hutter *The Dynamics of Avalanches of Granular Materials from Initiation to Runout. Part 1: Analysis*, Acta Mechanica (1991) vol. 86, pp. 201-223

[18] K. Hutter, Y. Wang & S.P. Pudasaini *The Savage-Hutter Avalanche Model. How Far Can it be Pushed?*, Philosophical Transactions A: Mathematical, Physical and Engineering Sciences, the Royal Society, London, Vol. 363(1832), 1507 - 1528

[19] Y.C Tai, S. Noelle, J.M.N.T Gray & K. Hutter *Shock-Capturing and Front-Tracking Methods for Granular Avalanches*, J. Comp. Phys. (2002) vol. 175, pp. 269-301

[20] ESSCC, University of Queensland, Computational Volcanology web pages, *shake200.esscc.uq.edu.au/twiki/bin/view/ESSCC/ComputationalPlanetaryScaleSimulation*